New Journal of Physics
The open-access journal for physics

Traffic jams induced by rare switching events in two-lane transport

Tobias Reichenbach[1], **Erwin Frey and Thomas Franosch**
Arnold Sommerfeld Center for Theoretical Physics (ASC)
and Center for NanoScience (CeNS), Department of Physics,
Ludwig-Maximilians-Universität München, Theresienstrasse 37,
D-80333, München, Germany
E-mail: tobias.reichenbach@physik.lmu.de

New Journal of Physics **9** (2007) 159
Received 6 February 2007
Published 4 June 2007
Online at http://www.njp.org/
doi:10.1088/1367-2630/9/6/159

Abstract. We investigate a model for driven exclusion processes where internal states are assigned to the particles. The latter account for diverse situations, ranging from spin states in spintronics to parallel lanes in intracellular or vehicular traffic. Introducing a coupling between the internal states by allowing particles to switch from one to another induces an intriguing polarization phenomenon. In a mesoscopic scaling, a rich stationary regime for the density profiles is discovered, with localized domain walls in the density profile of one of the internal states being feasible. We derive the shape of the density profiles as well as resulting phase diagrams analytically by a mean-field approximation and a continuum limit. Continuous as well as discontinuous lines of phase transition emerge, their intersections induce multi-critical behaviour.

[1] Author to whom any correspondence should be addressed.

PII: S1367-2630(07)43545-5

Contents

1. Introduction

Non-equilibrium critical phenomena arise in a broad variety of systems, including non-equilibrium growth models [1], percolation-like processes [2], kinetic Ising models [3], diffusion limited chemical reactions [4], and driven diffusive systems [5]. The latter provide models for transport processes ranging from biological systems, like the motion of ribosomes along a *m*-RNA chain [6] or processive motors walking along cytoskeletal filaments [7, 8], to vehicular traffic [9, 10]. In this work, we focus on the steady-state properties of such one-dimensional transport models, for which the totally asymmetric simple exclusion process (TASEP) has emerged as a paradigm (for reviews see e.g. [11]–[13]). There, particles move unidirectionally from left to right on a one-dimensional lattice, interacting through on-site exclusion. The entrance/exit rates at the open left/right boundary control the system's behaviour; tuning them, one encounters different non-equilibrium phases for the particle densities [14].

Intense theoretical research has been devoted to the classification of such non-equilibrium phenomena. For example, within the context of reaction–diffusion systems, there is strong evidence that phase transitions from an active to an absorbing state can be characterized in terms of only a few universality classes, the most important being the one of directed percolation (DP) [15]. To search for novel critical behaviour, fruitful results have been obtained by coupling two reaction–diffusion systems [16, 17], each undergoing the active to absorbing phase transition. Due to the coupling, the system exhibits a multi-critical point with unusual critical behaviour.

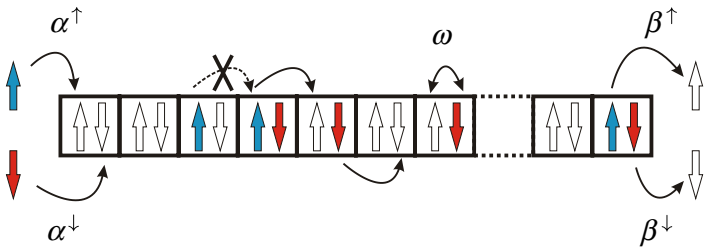

Figure 1. Illustration of an exclusion model with two internal states, adopting the language of spin transport. Particles in states $\uparrow$ ($\downarrow$) enter with rates $\alpha^{\uparrow}$ ($\alpha^{\downarrow}$), move unidirectionally to the right within the lattice, may flip at rate ω and leave the system at rates $\beta^{\uparrow}(\beta^{\downarrow})$, always respecting Pauli's exclusion principle.

We want to stress that already in equilibrium physics seminal insights have been gained by coupling identical systems. For instance, spin-ladders incorporate several Heisenberg spin chains [18]. There, quantum effects lead to a sensitive dependence on the chain number: for even ones a finite energy gap between the ground state and the lowest excitation emerges whereas gapless excitations dominate the low-temperature behaviour if the number of spin chains is odd.

In this work, we generalize the TASEP in a way that particles possess two internal states; we have recently published a short account of this work in [19]. Allowing particles to occasionally switch from one internal state to the other induces a coupling between the latter; indeed, the model may alternatively be regarded as two coupled TASEPs. When independent, each of them separately undergoes boundary-induced phase transitions [14]. The coupling is expected to induce novel phenomena, which are the subject of the present work.

Exclusion is introduced by allowing multiple occupancy of lattice sites only if particles are in different internal states. Viewing the latter as spin-1/2 states, i.e. spin-up ($\uparrow$) and spin-down ($\downarrow$), this directly translates into Pauli's exclusion principle; see figure 1. Indeed, the exclusion process presented in this work may serve as a model for semiclassical transport in mesoscopic quantum systems [20], like hopping transport in chains of quantum dots in the presence of an applied field [21]. Our model incorporates the quantum nature of the particles through Pauli's exclusion principle, though phase coherence is ignored. A surprising analogy to a simple spintronics scheme, the Datta–Das spin field-effect transistor [20], holds. There, electrons move unidirectionally through a ferromagnetic metal or a semiconductor. The polarization of the electrons is controllable by a source for spin injection, a drain for spin extraction as well as a gate in the form of a tunable magnetic field that controls the strength of spin precession. In our model, this is mimicked by considering the spin-flip rate as a control parameter.

The model is potentially relevant within biological contexts, as well. In intracellular traffic [7, 22], molecular motors walking on parallel filaments may detach from one lane and attach on another, resulting in an effective switching between the lanes. In our model, identifying the two internal states with different lanes, one recovers a transport model on two lanes with simple site exclusion. In the same way, the system presented in this work serves as a highly simplified cartoon model of multi-lane highway traffic taking lane switching into account [9, 10].

Significant insight into multi-lane traffic has been achieved (see [9, 10] and references therein). In particular, novel phases have been discovered in the case of indirect coupling, i.e. the velocity of the particles depends on the configuration on the neighbouring lane [23]–[25]. Recently, models have been presented that allow particles to switch between lanes, and the

transport properties have in part been rationalized in terms of an effective single lane TASEP [26]–[28]. There, the case of strong coupling has been investigated: the time-scale of lane switching events is the same as of forward hopping. In our model, we explicitly want to ensure a competition between the boundary processes and the switching between the internal states. We therefore employ a mesoscopic scaling, i.e. we consider the case where the switching events are rare as compared to forward hopping. This is the situation encountered in intracellular traffic [7] where motors nearly exclusively remain on one lane and switch only very rarely. In the context of spin transport, it corresponds to the case where forward hopping occurs much faster than spin precession (weak external magnetic field).

The outline of the present paper is the following. In section 2, we introduce the model in the context of spin transport as well as two-lane traffic. Symmetries and currents are discussed, which play a key role in the following analysis. Section 3 describes in detail the mean-field approximation and the differential equations for the densities obtained therefrom through a continuum limit. The mesoscopic scaling is motivated and introduced, the details of the analytic solution for the spatial density profiles being condensed in appendix A. We obtain the generic form of the density profiles in section 4, and compare our analytic results to stochastic simulations. We find that they agree excellently, suggesting the exactness of our analytic approach in the limit of large systems. As our main result, we encounter the polarization phenomenon, where the density profiles in the stationary non-equilibrium state exhibit localized 'shocks'. Namely, the density of one spin state changes abruptly from low-density (LD) to high-density (HD). The origin of this phenomenon is rationalized in terms of singularities in coupled differential equations. We partition the full parameter space into three distinct regions, and observe a delocalization transition. The methods to calculate the phase boundaries analytically are developed simultaneously. Section 5 presents details on the stochastic simulations which we have carried out to corroborate our analytic approach. The central result of this work is then addressed in section 6, where two-dimensional analytic phase diagrams are investigated. Our analytic approach identifies the phases where the polarization phenomenon occurs, as well as the continuous and discontinuous transitions that separate the phases. The nature of the transitions is explained by the injection/extraction limited current which is conserved along the track. As a second remarkable feature of the model, we uncover multi-critical points, i.e. points where two lines of phase boundaries intersect or the nature of a phase transition changes from discontinuous to a continuous one. Although multi-critical point are well-known in equilibrium statistical mechanics, a fundamental description for such a behaviour for systems driven far from equilibrium still constitutes a major challenge. A brief summary and outlook concludes this work.

2. The model

In this section, we describe our model in terms of spin transport as well as two-lane traffic. Though we will preferentially use the language of spins in the subsequent sections, the two-lane interpretation is of no lesser interest, and straightforwardly obtained. Furthermore, we introduce two symmetries which are manifest on the level of the dynamical rules.

2.1. Dynamical rules

We consider hopping transport on a one-dimensional lattice, composed of L sites, with open boundaries, see figure 1. Particles possess internal states, which we restrict to two different

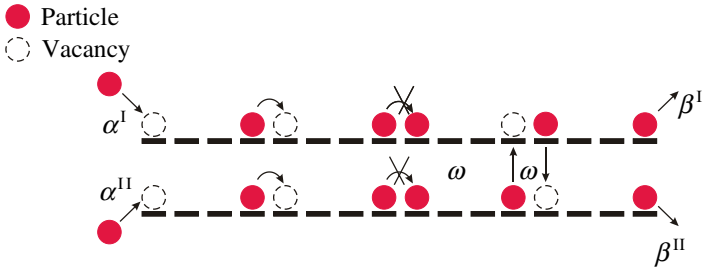

Figure 2. Illustration of the two-lane interpretation. We label the upper lane as lane I and the lower one as lane II. They possess individual entering rates, α^{I} resp. α^{II} as well as exiting rates, β^{I} resp. β^{II}.

kinds; adopting a spin notation, they are referred to as spin-up ($\uparrow$) and spin-down ($\downarrow$). They enter at the left boundary at rates $\alpha^{\uparrow}$ resp. $\alpha^{\downarrow}$, and move unidirectionally from left to the right through the lattice. The time-scale is fixed by putting the rate for these hopping events to unity. Within the bulk, particles may also flip their spin state, from spin-up to spin-down and back, at rate ω. Finally, having reached the right boundary, particles may exit the system at rates $\beta^{\uparrow}$ resp. $\beta^{\downarrow}$, depending on their spin state. We allow all of these processes only under the constraint of Pauli's exclusion principle, meaning that every lattice site may at most be occupied by one particle of a given state. Spin-up and spin-down thus may simultaneously occupy the same site, however two particles with identical spin polarization cannot share a lattice site. In summary, our dynamical rules are the following:

i. at site $i = 1$ (left boundary), particles with spin-up (spin-down) may enter at rate $\alpha^{\uparrow}(\alpha^{\downarrow})$,
ii. at site $i = L$ (right boundary), particles with spin-up (spin-down) leave the lattice at rate $\beta^{\uparrow}(\beta^{\downarrow})$,
iii. particles may hop at unit rate from site $i - 1$ to the neighbouring site i for $i \in \{2, \ldots, L\}$, i.e. within bulk,
iv. within bulk, particles can flip their spin state with rate ω, i.e. spin-up turns into spin-down and vice versa,

always respecting Pauli's exclusion principle. Processes (i)–(iii) constitute the TASEP for the two different states separately, while rule (iv) induces a coupling between them. Indeed, when the spin-flip rate ω vanishes, we recover the trivial situation of two independent TASEPs, while we will show that a proper treatment of ω through a mesoscopic scaling induces nontrivial effects.

2.2. Two-lane interpretation

Having introduced our model in the language of semi-classical spin transport, where Pauli's exclusion principle is respected while phase coherence completely ignored, we now want to show that it also describes transport with site exclusion on two parallel lanes. As schematically drawn in figure 2, we consider two parallel lanes, each consisting of L sites, labelled as upper lane (I) and lower lane (II). They are identified with the internal states of the particles considered before: a particle with spin-up (spin-down) now corresponds to a particle on lane I (lane II). The processes (i) and (ii) describe entering of particles at lane I (II) at rate $\alpha^{\mathrm{I}} \equiv \alpha^{\uparrow}$ ($\alpha^{\mathrm{II}} \equiv \alpha^{\downarrow}$)

and exiting of lane I (II) at rate $\beta^{\mathrm{I}} \equiv \beta^{\uparrow}$ ($\beta^{\mathrm{II}} \equiv \beta^{\downarrow}$). Due to (iii), particles hop unidirectionally to the right on each individual lane; at rate ω, they may switch from lane I to II and back. Pauli's exclusion principle translates into simple site exclusion: all the above processes are allowed under the constraint of admitting at most one particle per site. Again, we clearly observe that it is process (iv) that couples two TASEPs, namely the ones on each individual lane, to each other.

2.3. Symmetries

Already on the level of the dynamical rules (i)–(iv) presented above, two symmetries are manifest that will prove helpful in the analysis of the system's behaviour. We refer to the absence of particles with certain state as holes with the opposite respective state[2]. Considering their motion, we observe that the dynamics of the holes is governed by the identical rules (i)–(iv), with 'left' and 'right' interchanged, i.e. with a discrete transformation of sites $i \leftrightarrow L - i$ as well as rates $\alpha^{\uparrow,\downarrow} \leftrightarrow \beta^{\downarrow,\uparrow}$. The system thus exhibits a *particle–hole symmetry*. Even more intuitively, the two states behave qualitatively identical. Indeed, the system remains invariant upon changing spin-up to spin-down states and vice versa with a simultaneous interchange of $\alpha^{\uparrow} \leftrightarrow \alpha^{\downarrow}$ and $\beta^{\uparrow} \leftrightarrow \beta^{\downarrow}$, constituting a *spin symmetry* (in terms of the two-lane interpretation, it translates into a *lane symmetry*).

When analysing the system's behaviour in the five-dimensional phase space, constituted of the entrance and exit rates $\alpha^{\uparrow,\downarrow}$, $\beta^{\uparrow,\downarrow}$ and ω, these symmetries allow to connect different regions in phase space, and along the way to simplify the discussion.

3. Mean-field equations, currents and the continuum limit

In this section, we shall make use of the dynamical rules introduced above to set up a quantitative description for the densities and currents in the system. Within a mean-field approximation, their time evolution is expressed through one-point functions only, namely the average occupations of a lattice site. Such mean-field approximations have been successfully applied to a variety of driven diffusive systems, see e.g. [12]. We focus on the properties of the non-equilibrium steady state, which results from boundary processes (entering and exiting events) as well as bulk ones (hopping and spin-flip events). Both types of processes compete if their time-scales are comparable; we ensure this condition by introducing a *mesoscopic scaling* for the spin flip rate ω. Our focus is on the limit of large system sizes L, which is expected to single out distinct phases. To solve the resulting equations for the densities and currents, a continuum limit is then justified, and it suffices to consider the leading order in the small parameter, namely the ratio of the lattice constant to system size. Such a mesoscopic scaling has been already successfully used in [29, 30] in the context of TASEP coupled to Langmuir dynamics.

3.1. Mean field approximation and currents

Let $n_i^{\uparrow}(t)$ resp. $n_i^{\downarrow}(t)$ be the fluctuating occupation number of site i for spin-up resp. spin-down state, i.e. $n_i^{\uparrow,\downarrow}(t) = 1$ if this site is occupied at time t by a particle with the specified spin state and $n_i^{\uparrow,\downarrow}(t) = 0$ otherwise. Performing ensemble averages, the expected occupation, denoted by $\rho_i^{\uparrow}(t)$

[2] The convention to flip the spin simultaneously is natural in the language of solid-state physics. In the context of two-lane traffic, it appears more natural to consider vacancies moving on the *same* lane in the reverse direction.

and $\rho_i^{\downarrow}(t)$, is obtained. Within a mean-field approximation, higher order correlations between the occupation numbers are neglected, i.e. we impose the factorization approximation

$$\langle n_i^r(t) n_j^s(t)\rangle = \rho_i^r(t)\rho_j^s(t); \quad r, s \in \{\uparrow, \downarrow\}. \tag{1}$$

Equations of motion for the densities can by obtained via *balance equations*. The time-change of the density at a certain site is related to appropriate currents. The spatially varying *spin current* $j_i^{\uparrow}(t)$ quantifies the rate at which particles of spin state $\uparrow$ at site $i-1$ hop to the neighbouring site i. Within the mean-field approximation, equation (1), the current is expressed in terms of densities as

$$j_i^{\uparrow}(t) = \rho_{i-1}^{\uparrow}(t)[1-\rho_i^{\downarrow}(t)], \qquad i \in \{2, \ldots, L\}, \tag{2}$$

and similarly for the current $j_i^{\downarrow}(t)$. The sum yields the total *particle current* $J_i(t) \equiv j_i^{\uparrow}(t) + j_i^{\downarrow}(t)$. Due to the spin-flip process (iv), there also exists a *leakage current* $j_i^{\uparrow\downarrow}(t)$ from spin-up state to spin-down state. Within mean-field

$$j_i^{\uparrow\downarrow}(t) = \omega\rho_i^{\uparrow}(t)[1-\rho_i^{\downarrow}(t)], \tag{3}$$

and similarly for the leakage current $j_i^{\downarrow\uparrow}(t)$ from spin-down to spin-up state. Now, for $i \in \{2, \ldots, L-1\}$ we can use balance equations to obtain the time evolution of the densities,

$$\frac{\mathrm{d}}{\mathrm{d}t}\rho_i^{\uparrow}(t) = j_i^{\uparrow}(t) - j_{i+1}^{\uparrow}(t) + j_i^{\downarrow\uparrow}(t) - j_i^{\uparrow\downarrow}(t). \tag{4}$$

This constitutes an exact relation. Together with the mean field approximation for the currents, equations (2) and (3), one obtains a set of closed equations for the local densities

$$\frac{\mathrm{d}}{\mathrm{d}t}\rho_i^{\uparrow}(t) = \rho_{i-1}^{\uparrow}(t)[1-\rho_i^{\uparrow}(t)] - \rho_i^{\uparrow}(t)[1-\rho_{i+1}^{\uparrow}(t)] + \omega\rho_i^{\downarrow}(t) - \omega\rho_i^{\uparrow}(t). \tag{5}$$

At the boundaries of the track, the corresponding expressions involve also the entrance and exit events, which are again treated in the spirit of a mean-field approach

$$\frac{\mathrm{d}}{\mathrm{d}t}\rho_1^{\uparrow}(t) = \alpha^{\uparrow}[1-\rho_1^{\uparrow}(t)] - \rho_1^{\uparrow}(t)[1-\rho_2^{\uparrow}(t)] + \omega\rho_1^{\downarrow}(t) - \omega\rho_1^{\uparrow}(t), \tag{6}$$

$$\frac{\mathrm{d}}{\mathrm{d}t}\rho_L^{\uparrow}(t) = \rho_{L-1}^{\uparrow}(t)[1-\rho_L^{\uparrow}(t)] - \beta^{\uparrow}\rho_L^{\uparrow}(t) + \omega\rho_L^{\downarrow}(t) - \omega\rho_L^{\uparrow}(t). \tag{7}$$

Due to the spin symmetry, i.e. interchanging $\uparrow$ and $\downarrow$, an analogous set of equations holds for the time evolution of the density of particles with spin-down state.

In the stationary state, the densities $\rho_i^{\uparrow(\downarrow)}(t)$ do not depend on time t, such that the time derivatives in equations (5)–(7) vanish. Therefrom, we immediately derive the spatial conservation of the particle current: indeed, summing equation (4) with the corresponding equation for the density of spin-down states yields

$$J_i = J_{i+1}, \qquad i \in \{2, \ldots, L-1\}, \tag{8}$$

such that the particle current does not depend on the spatial position i. Note that this does not apply to the individual spin currents, they *do* have a spatial dependence arising from the leakage currents.

In a qualitative discussion, let us now anticipate the effects that arise from the non-conserved individual spin currents as well as from the conserved particle current. The latter has its analogy in TASEP, where the particle current is spatially conserved as well. It leads to two distinct regions in the parameter space: one where the current is determined by the left boundary, and the other where it is controlled by the right one. Both regions are connected by the discrete particle–hole symmetry. Thus, in general, discontinuous phase transitions arise when crossing the border from one region to the other. In our model, we will find similar behaviour: the particle current is either determined by the left or by the right boundary. Again, both regions are connected by the discrete particle–hole symmetry, such that we expect discontinuous phase transitions at the border between both. Except for a small, particular region in the parameter space, this behaviour is captured quantitatively by the mean-field approach and the subsequent analysis, which is further corroborated by stochastic simulations. The phenomena linked to the particular region will be presented elsewhere [31].

On the other hand, the non-conserved spin currents may be compared to the current in TASEP coupled to Langmuir kinetics, see [29, 30]. Due to attachment and detachment processes, the in-lane current is only weakly conserved, allowing for a novel phenomenon, namely phase separation into a LD and a HD region separated by a localized domain wall. The transitions to this phase are continuous considering the domain wall position x_w as the order parameter. In our model, an analogous but even more intriguing phase will appear as well, with continuous transitions being possible.

3.2. Mesoscopic scaling and the continuum limit

3.2.1. Mesoscopic scaling. Phases and corresponding phase transitions are expected to emerge in the limit of large system size, $L \to \infty$, which therefore constitutes the focus of this work. We expect interesting phase behaviour to arise from the coupling of spin-up and spin-down states via spin-flip events, in addition to the entrance and exit processes. Clearly, if spin-flips occur on a fast time-scale, comparable to the hopping events, the spin degree of freedom is relaxed, such that the system's behaviour is effectively the one of a TASEP. Previous work on related two-lane models [27, 26] focused on the physics in that situation. In this work, we want to highlight the dynamical regime where coupling through spin-flips is present, however not sufficiently strong to relax the system's internal degree of freedom. In other words, we consider physical situations where spin-flips occur on the same time-scale as the entrance/exit processes. Defining the *gross* spin-flip rate $\Omega = \omega L$ yields a measure of how often a particle flips its spin state while traversing the system. To ensure competition between spin-flips with boundary processes, a *mesoscopic scaling* of the rate ω is employed by keeping Ω fixed, of the same order as the entrance/exit rates, when the number of lattice sites becomes large $L \to \infty$.

3.2.2. Continuum limit and first order approximation. The total length of the lattice will be fixed to unity and one may define consistently the lattice constant $\epsilon = 1/L$. In the limit of large systems $\epsilon \to 0$, a *continuum limit* is anticipated. We introduce continuous functions $\rho^{\uparrow}(x)$ resp. $\rho^{\downarrow}(x)$ through $\rho^{\uparrow}(x_i) = \rho_i^{\uparrow}$ resp. $\rho^{\downarrow}(x_i) = \rho_i^{\downarrow}$ at the discrete points $x_i = \mathrm{i}\epsilon$. Expanding these to

first order in the lattice constant,

$$\rho^{\uparrow(\downarrow)}(x_{i\pm1}) = \rho^{\uparrow(\downarrow)}(x_i \pm \epsilon) = \rho^{\uparrow(\downarrow)}(x_i) \pm \epsilon\partial_x\rho^{\uparrow(\downarrow)}(x_i), \tag{9}$$

the difference equations (5)–(7) turn into differential equations. Observing that $\omega = \epsilon\Omega$ is already of order ϵ, we find that the zeroth order of equation (5) vanishes, and the first order in ϵ yields

$$[2\rho^{\uparrow}(x) - 1]\partial_x\rho^{\uparrow}(x) + \Omega\rho^{\downarrow}(x) - \Omega\rho^{\uparrow}(x) = 0. \tag{10}$$

Similarly, the same manipulations for $\rho^{\downarrow}$ yield

$$[2\rho^{\downarrow}(x) - 1]\partial_x\rho^{\downarrow}(x) + \Omega\rho^{\uparrow}(x) - \Omega\rho^{\downarrow}(x) = 0. \tag{11}$$

The expansion of equations (6) and (7) in powers of ϵ, yields in zeroth order

$$\begin{aligned} \rho^{\uparrow}(0) &= \alpha^{\uparrow}, \qquad \rho^{\uparrow}(1) = 1 - \beta^{\uparrow}, \\ \rho^{\downarrow}(0) &= \alpha^{\downarrow}, \qquad \rho^{\downarrow}(1) = 1 - \beta^{\downarrow}, \end{aligned} \tag{12}$$

which impose *boundary conditions*. Since two boundary conditions are enough to specify a solution of the coupled first-order differential equations, the system is apparently over-determined. Of course, the full analytic solution, i.e. where all orders in ϵ are incorporated, will be only *piecewise* given by the first-order approximation, equations (10)–(12). Between these branches, the solution will depend on higher-orders of ϵ, therefore, these intermediate regions scale with order ϵ and higher. They vanish in the limit of large systems, $\epsilon \to 0$, yielding *domain walls* or *boundary layers*.

Let us explain the latter terms. At the position of a domain wall, situated in bulk, the density changes its value discontinuously, from one of a LD region to one of a HD. Boundary layers are pinned to the boundaries of the system. There as well, the density changes discontinuously: from a value that is given by the corresponding boundary condition to that of a LD or HD region which is imposed by the opposite boundary.

3.2.3. Symmetries and currents revisited. In the following, we reflect important properties of the system, symmetries and currents, on the level of the first-order approximation, equations (10)–(12). The explicit solution of the latter can be found in appendix A.

The particle–hole symmetry, already inferred from the dynamical rules, now takes the form

$$\rho^{\uparrow(\downarrow)}(x) \leftrightarrow 1 - \rho^{\uparrow(\downarrow)}(1 - x), \qquad \alpha^{\uparrow(\downarrow)} \leftrightarrow \beta^{\uparrow(\downarrow)}. \tag{13}$$

Interchanging $\uparrow$ and $\downarrow$ in the densities as well as the in and outgoing rates yields the spin symmetry,

$$\rho^{\uparrow}(x) \leftrightarrow \rho^{\downarrow}(x), \qquad \alpha^{\uparrow} \leftrightarrow \alpha^{\downarrow}, \qquad \beta^{\uparrow} \leftrightarrow \beta^{\downarrow}. \tag{14}$$

The individual spin currents as well as the particle current have been anticipated to provide further understanding of the system's behaviour. In the continuum limit the zeroth order of the spin currents is found to be $j^{\uparrow(\downarrow)}(x) = \rho^{\uparrow(\downarrow)}(x)[1 - \rho^{\uparrow(\downarrow)}(x)]$, such that equations (10), (11) may

be written in the form

$$\partial_x j^{\uparrow} = \Omega[\rho^{\downarrow} - \rho^{\uparrow}], \quad \partial_x j^{\downarrow} = \Omega[\rho^{\uparrow} - \rho^{\downarrow}]. \tag{15}$$

The terms on the right-hand side, arising from the spin-flip process (iv), are seen to violate the spatial conservation of the spin currents. However, due to the mesoscopic scaling of the spin flip rate ω, the leakage currents between the spin states are only weak, see equation (3), locally tending to zero when $\epsilon \to 0$, such that the spin currents vary *continuously* in space. This finding imposes a condition for the transition from one branch of first-order solution to another, as described above: such a transition is only allowed when the corresponding spin currents are continuous at the transition point, thus singling out distinct positions for a possible transition.

Finally, summing the two equations in equation (15) yields the spatial conservation of the particle current: $\partial_x J = 0$.

4. Partition of the parameter space and the generic density behaviour

The parameter space of our model, spanned by the five rates $\alpha^{\uparrow,\downarrow}$, $\beta^{\uparrow,\downarrow}$, and Ω, is of high dimensionality. However, in this section, we show that it can be decomposed into only three basic distinct regions: the maximal-current (MC) region as well as the injection-limited (IN) and the extraction-limited one (EX). While trivial phase behaviour occurs in the MC region, our focus is on the IN and EX region (connected by particle–hole symmetry), where a striking polarization phenomenon occurs. The generic phase behaviour in these regions is derived, exhibiting this effect.

4.1. Effective rates

The entrance and exit rates as well as the carrying capacity of the bulk impose restrictions on the particle current. For example, the capacity of the bulk limits the individual spin currents $j^{\uparrow(\downarrow)}$ to maximal values of $1/4$. The latter occurs at a density of $1/2$, as seen from the previous result $j^{\uparrow(\downarrow)} = \rho^{\uparrow(\downarrow)}[1 - \rho^{\uparrow(\downarrow)})]$. To illustrate the influence of the injection and extraction rates, we first consider an 'open' right boundary i.e. $\beta^{\uparrow} = \beta^{\downarrow} = 1$. Particles then leave the system unhindered, such that only the entrance rates may limit the particle current. Provided one of these rates, say $\alpha^{\uparrow}$, exceeds the value $1/2$, the current of the corresponding state ($\uparrow$) is limited by the capacity of the bulk to a value of $1/4$ in the vicinity of the left boundary. A boundary layer thus forms in the density profile of spin-up state at the left boundary, connecting the value of the injection rate $\alpha^{\uparrow}$ to the value $1/2$. Up to this boundary layer, the density profile $\rho^{\uparrow}(x)$ is identical to the one where $\alpha^{\uparrow}$ takes a value of $1/2$, cf figure 3. Similar reasoning holds for the extraction rates $\beta^{\uparrow(\downarrow)}$. They as well behave effectively as $1/2$ when exceeding this value. To treat these findings properly, we introduce the *effective rates*

$$\alpha_{\mathrm{eff}}^{\uparrow(\downarrow)} = \min\left[\alpha^{\uparrow(\downarrow)}, \tfrac{1}{2}\right], \tag{16a}$$

$$\beta_{\mathrm{eff}}^{\uparrow(\downarrow)} = \min\left[\beta^{\uparrow(\downarrow)}, \tfrac{1}{2}\right]. \tag{16b}$$

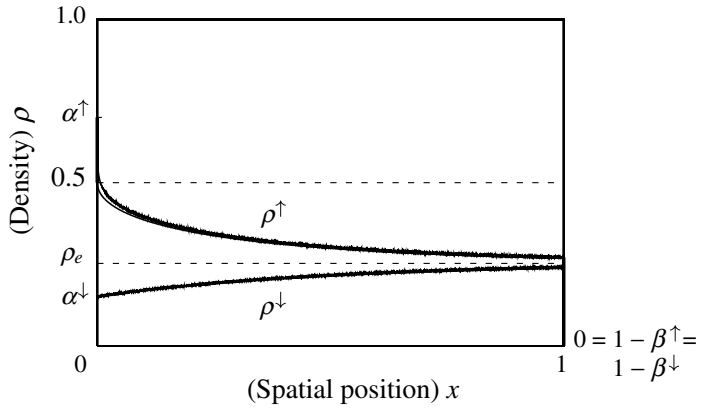

Figure 3. Illustration of the effective rates. The right boundary is 'open', such that only the capacity of the bulk and the entrance rates limit the spin currents. The injection rate $\alpha^{\uparrow} > \frac{1}{2}$ effectively acts as $\frac{1}{2}$. The analytic predictions correspond to the solid lines, the results from stochastic simulations for $L = 10\,000$ are indicated by the wiggly line. With increasing spatial position, the densities approach a common value ρ_e. The parameters used are $\alpha^{\uparrow} = 0.7$, $\alpha^{\downarrow} = 0.15$ and $\Omega = 0.5$.

The system's bulk behaviour will only depend on them, and, in particular, remain unaffected when a rate is varied at values exceeding $1/2$.

4.2. IN, EX, and MC region

Equipped with these results, in the case of an 'open' right boundary, the spin currents in the vicinity of the left boundary are given by $j^{\uparrow} = \alpha^{\uparrow}_{\mathrm{eff}}(1 - \alpha^{\uparrow}_{\mathrm{eff}})$ resp. $j^{\downarrow} = \alpha^{\downarrow}_{\mathrm{eff}}(1 - \alpha^{\downarrow}_{\mathrm{eff}})$, resulting in a particle current J_{IN} imposed by the injection rates: $J_{\mathrm{IN}} = \alpha^{\uparrow}_{\mathrm{eff}}(1 - \alpha^{\uparrow}_{\mathrm{eff}}) + \alpha^{\downarrow}_{\mathrm{eff}}(1 - \alpha^{\downarrow}_{\mathrm{eff}})$. The analogous relations, with the injection and extraction rates interchanged, hold for the case of an 'open' left boundary, $\alpha^{\uparrow} = \alpha^{\downarrow} = 1$. The particle current is then controlled by the right boundary: $J_{\mathrm{EX}} = \beta^{\uparrow}_{\mathrm{eff}}(1 - \beta^{\uparrow}_{\mathrm{eff}}) + \beta^{\downarrow}_{\mathrm{eff}}(1 - \beta^{\downarrow}_{\mathrm{eff}})$. In general, depending on which imposes the stronger restriction, either the left or the right boundary limits the particle current: $J \leqslant \min(J_{\mathrm{IN}}, J_{\mathrm{EX}})$. Indeed, $J = \min(J_{\mathrm{IN}}, J_{\mathrm{EX}})$ holds except for an anomalous situation, where the current is lower than this value[3]. Depending on which of both cases applies, two complementary regions in phase space are distinguished: $J_{\mathrm{IN}} < J_{\mathrm{EX}}$ is termed IN *region*, while $J_{\mathrm{IN}} > J_{\mathrm{EX}}$ defines the EX *region*. Since they are connected by discrete particle–hole symmetry, we expect *discontinuous phase transitions* across the border between both, to be referred as IN–EX boundary.

Right at the IN–EX boundary, the system exhibits coexistence of LD and HD phases, separated by domain walls. Interestingly, this phase coexistence emerges on *both* lanes (states), which may be seen as follows. Recall that a domain wall concatenates a region of low and another of HD. However, while the densities exhibit a discontinuity, the spin currents must be continuous. In other words, the spin currents, and therefore the particle currents, imposed by the left and right boundary must match each other. This yields the condition $J_{\mathrm{IN}} = J_{\mathrm{EX}}$, which is nothing but the relation describing the IN–EX boundary. Actually, what we have shown with this argument is that domain walls on both lanes (states) are *at most* feasible at the IN–EX boundary. However,

[3] This situation arises in a certain neighbourhood of the multi-critical points $\mathcal{B}$, discussed in section 6.

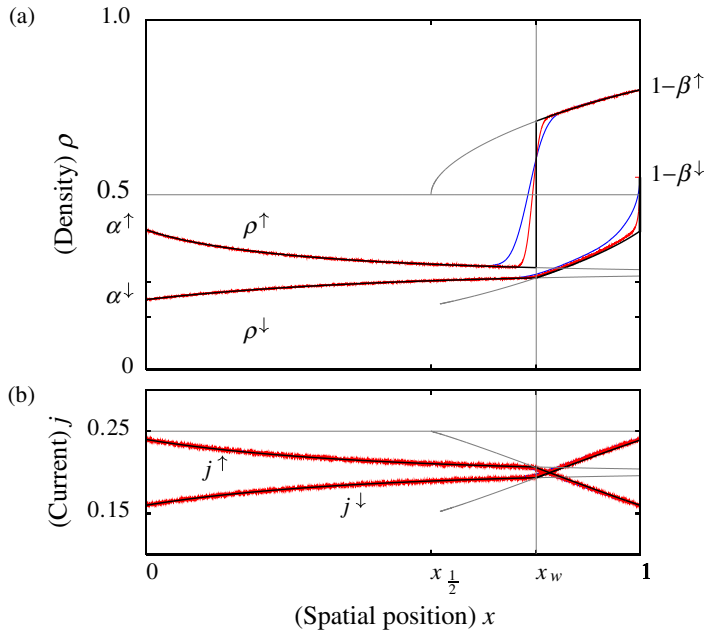

Figure 4. The densities (a) and currents (b) in the IN region: generic state, exhibiting the polarization phenomenon. Results from stochastic simulations are shown as blue ($L = 2000$) resp. red ($L = 10\,000$) lines. They piecewise obey the first-order approximations (black), grey lines indicate continuations of the latter into regions where the densities are no longer given by them. The parameters are $\alpha^{\uparrow} = 0.4$, $\alpha^{\downarrow} = 0.2$, $\beta^{\uparrow} = 0.2$, $\beta^{\downarrow} = 0.45$, and $\Omega = 0.5$.

it turns out that there, they do indeed form, and are delocalized. We refer to our forthcoming publication [31] for a detailed discussion of this phenomenon. Away from the IN–EX boundary, it follows that at most on one lane (state) a domain wall may appear.

When both entrance rates $\alpha^{\uparrow}$, $\alpha^{\downarrow}$ as well as both exit rates $\beta^{\uparrow}$, $\beta^{\downarrow}$ exceed the value $1/2$, the particle current is limited by neither boundary, but only through the carrying capacity of the bulk, restricting it to twice the maximal value $1/4$ of the individual spin currents: $J = 1/2$. The latter situation therefore constitutes the *maximal current region*.

4.3. The generic state of the densities

As we have seen in the previous section, particularly simple density profiles emerge in the MC region. There, up to boundary layers, the density profiles remain constant at a value $1/2$ for each spin state. Another special region in parameter space is the IN–EX boundary, characterized by the simultaneous presence of domain walls in both spin states, as we discuss elsewhere [31].

Away from these regions, the generic situation for the density profiles is illustrated in figure 4. Here, we have considered parameters belonging to the IN region; the behaviour in the EX region follows from particle–hole symmetry. A domain wall emerges for one spin state and a boundary layer for the other one. For specificity, we consider a domain wall for the spin-up state, the other situation is obtained from spin symmetry. The density profiles $\rho_{\mathrm{l}}^{\uparrow(\downarrow)}$ close to the left boundary are given by the solution of the first-order differential equations (10) and (11), obeying the left boundary conditions $\rho_{\mathrm{l}}^{\uparrow}(x = 0) = \alpha_{\mathrm{eff}}^{\uparrow}$ and $\rho_{\mathrm{l}}^{\downarrow}(x = 0) = \alpha_{\mathrm{eff}}^{\downarrow}$. For the density profiles $\rho_{\mathrm{r}}^{\uparrow(\downarrow)}$ in

the vicinity of the right boundary, we use the fact that the current in bulk is determined by the injection rates, $J = J_{\mathrm{IN}}$ (which defines the IN region). Therefore, the densities satisfy right boundary conditions which are given by $\rho_{\mathrm{r}}^{\uparrow}(x = 1) = 1 - \beta_{\mathrm{eff}}^{\uparrow}$; and $\rho_{\mathrm{r}}^{\downarrow}(x = 1)$ is found from the conservation of the particle current:

$$J = \alpha_{\mathrm{eff}}^{\uparrow}(1 - \alpha_{\mathrm{eff}}^{\uparrow}) + \alpha_{\mathrm{eff}}^{\downarrow}(1 - \alpha_{\mathrm{eff}}^{\downarrow}) = \beta_{\mathrm{eff}}^{\uparrow}(1 - \beta_{\mathrm{eff}}^{\uparrow}) + \rho_{\mathrm{r}}^{\downarrow}(x = 1)[1 - \rho_{\mathrm{r}}^{\downarrow}(x = 1)]. \tag{17}$$

At some point x_{w} in bulk, the left and right solutions have to be concatenated by a domain wall for spin-up. To determine the position x_{w} of this domain wall, we use the *continuity* of the spin currents; see figure 4(b)[4]. This continuity condition singles out a distinct spatial position for the domain wall: denote by $\rho_{\mathrm{l}}^{\uparrow}(x_{\mathrm{w}})$ the value of the density to the left of x_{w}, and $\rho_{\mathrm{r}}^{\uparrow}(x_{\mathrm{w}})$ the value to the right. From $j^{\uparrow} = \rho^{\uparrow}(1 - \rho^{\uparrow})$ together with $\rho_{\mathrm{l}}^{\uparrow}(x_{\mathrm{w}}) \neq \rho_{\mathrm{r}}^{\uparrow}(x_{\mathrm{w}})$, we arrive at the condition

$$\rho_{\mathrm{l}}^{\uparrow}(x_{\mathrm{w}}) = 1 - \rho_{\mathrm{r}}^{\uparrow}(x_{\mathrm{w}}) \tag{18}$$

for the domain wall position[5]. From the conservation of the particle current J, it follows that the density $\rho^{\downarrow}$ is continuous at the position x_{w}.

When considering the internal states as actual spins, the appearance of a domain wall in the density profile of one of the spin states results in a *spontaneous polarization phenomenon*. Indeed, while both the density of spin-up and spin-down remain at comparable low values in the vicinity of the left boundary, this situation changes upon crossing the point x_{w}. There, the density of spin-up jumps to a high value, while the density of spin-down remains at a low value, resulting in a polarization in this region.

Comparing the generic phase behaviour to the one of TASEP, we observe that the IN region can be seen as the analogue to the LD region there: within both, a LD phase accompanied by a boundary layer at the right boundary arises. Following these lines, the EX region has its analogue in the HD region, while the MC region is straightforwardly generalized from the one of TASEP. Furthermore, the delocalization transition across the IN–EX boundary is similar to the appearance of a delocalized domain wall at the coexistence line in TASEP.

4.4. Phases and phase boundaries

In the generic situation of figure 4, the density of spin-down is in a homogeneous LD state, while for spin-up, a LD and a HD region coexist. We refer to the latter as the LD–$\mathrm{HD}_{\mathrm{IN}}$ phase, as the phase separation arises within the IN region, to be contrasted from a LD–$\mathrm{HD}_{\mathrm{EX}}$ phase which may arise within the EX region. Clearly, the LD–$\mathrm{HD}_{\mathrm{IN}}$ phase is only present if the position x_{w} of the domain wall lies within bulk. Tuning the system's parameter, it may leave the system through the left or right boundary, resulting in a homogeneous phase. Indeed, $x_{\mathrm{w}} = 1$ marks the transition between the LD–$\mathrm{HD}_{\mathrm{IN}}$ phase and the pure LD state, while at $x_{\mathrm{w}} = 0$ the density changes from the LD–$\mathrm{HD}_{\mathrm{IN}}$ to a homogeneous HD state. Regarding the domain wall position x_{w} as an order parameter, these transitions are continuous. Implicit analytic expressions for these

[4] Indeed, though they are not spatially conserved, the mesoscopic scaling of the spin-flip rate ω was seen to cause a only slowly varying spatial dependence; in the continuum limit, the spin currents are continuous.

[5] For TASEP-like transport the particle–hole symmetry restricts the density jump to this mirror relation. More general current-density relations are feasible [32, 33], but are not expected to change the picture qualitatively.

phase boundaries, derived in the following, are obtained from the first-order approximation, equations (10) and (11).

Spin symmetry yields the analogous situation with a domain wall appearing in the density profile of spin-down, while particle–hole symmetry maps it to the EX region, where a pure HD phase arises for one of the spins. Discontinuous transitions accompanied by delocalized domain walls appear at the submanifold of the IN–EX boundary (see [31] for a detailed discussion).

The phase boundaries may be computed from the condition $x_w = 0$ and $x_w = 1$ in the situation of figure 4. Consider first the case of $x_w = 0$. There, the density profiles are fully given by the first-order approximation $\rho_r^{\uparrow(\downarrow)}$ satisfying the boundary conditions at the right. The condition (18) translates to

$$\rho_r^{\uparrow}(x = 0) = 1 - \rho_l^{\uparrow}(x = 0) = 1 - \alpha_{\text{eff}}^{\uparrow} \tag{19}$$

which yields an additional constraint on the system's parameters. This defines the hyper-surface in the IN region where $x_w = 0$ occurs, and thus the phase boundary between the LD–HD_{IN} and the pure HD phase.

Similarly, if $x_w = 1$, the densities follow the left solution $\rho_l^{\uparrow(\downarrow)}(x)$, determined by the left boundary conditions, within the whole system. From equation (18) we obtain

$$\rho_l^{\uparrow}(x = 1) = 1 - \rho_r^{\uparrow}(x = 1) = \beta_{\text{eff}}^{\uparrow}. \tag{20}$$

Again, the latter is a constraint on the parameters and defines the hyper-surface in the IN region where $x_w = 1$ is found, being the phase boundary between the LD–HD_{IN} and the homogeneous LD phase.

The conditions (19) and (20) yield implicit equations for the phase boundaries. The phase diagram is thus determined up to solving algebraic equations, which may be achieved numerically. Further insight concerning the phase boundaries is possible and may be obtained analytically, which we discuss next.

Firstly, we note that in the case of equal injection rates, $\alpha^{\uparrow} = \alpha^{\downarrow}$, the density profiles in the vicinity of the left boundary are constant. If in addition $\alpha^{\uparrow} = \alpha^{\downarrow} = \beta^{\uparrow} < 1/2$, we observe from equation (20) that a domain wall at $x_w = 1$ emerges. Therefore, this set of parameters always lies on the phase boundary $x_w = 1$, independent of the value of Ω.

Secondly, we investigate the phase boundary determined by $x_w = 0$. Comparing with figure 4, we observe that the first-order approximation $\rho_r^{\uparrow}$ for the density of spin-up may reach the value $\frac{1}{2}$ at a point which is denoted by $x_{1/2}$: $\rho_r^{\uparrow}(x_{1/2}) = \frac{1}{2}$. This point corresponds to a branching point of the first-order solution. Increasing Ω, the value of $x_{1/2}$ increases as well. The domain wall in the density of spin-up can only emerge at a value $x_w \geqslant x_{1/2}$. At most, $x_w = x_{1/2}$, in which case a domain wall with infinitesimal small height arises. For the phase boundary specified by $x_w = 0$, this implies that it only exists as long as $x_{1/2} \leqslant 0$. The case $x_w = x_{1/2} = 0$ corresponds to a domain wall of infinitesimal height, which is only feasible if $\alpha_{\text{eff}}^{\uparrow} = \frac{1}{2}$. Now, for given rates $\alpha_{\text{eff}}^{\uparrow} = \frac{1}{2}$, $\alpha^{\downarrow}$, $\beta^{\uparrow}$, the condition $x_{1/2} = 0$ yields a critical rate $\Omega^*(\alpha^{\downarrow}, \beta^{\uparrow})$, depending on the rates $\alpha^{\downarrow}$, $\beta^{\uparrow}$. The situation $x_w = 0$ can only emerge for rates $\Omega \leqslant \Omega^*(\alpha^{\downarrow}, \beta^{\uparrow})$. Varying the rates $\alpha^{\uparrow}$, $\alpha^{\downarrow}$ and $\beta^{\uparrow}$, the critical rate $\Omega^*(\alpha^{\downarrow}, \beta^{\uparrow})$ changes as well. In appendix A, we show that its largest value occurs at $\alpha^{\downarrow} = \beta^{\uparrow} = 0$. They yield the rate $\Omega_C \equiv \Omega^*(\alpha^{\downarrow} = \beta^{\uparrow} = 0)$, which is calculated to be

$$\Omega_C = 1 + \tfrac{1}{4}\sqrt{2}\ln(3 - 2\sqrt{2}) \approx 0.38. \tag{21}$$

The critical $\Omega^*(\alpha^\downarrow, \beta^\uparrow)$ are lying in the interval between 0 and Ω_C: $\Omega^*(\alpha^\downarrow, \beta^\uparrow) \in [0, \Omega_C]$, and all values in this interval in fact occur. The rate Ω_C defines a *scale* in the spin-flip rate Ω: For $\Omega \leqslant \Omega_C$, the phase boundary determined by $x_w = 0$ exists, while disappearing for $\Omega > \Omega_C$.

Thirdly, we study the form of the phase boundaries for large Ω, meaning $\Omega \gg \Omega_C$. In this case, the phase boundary specified by $x_w = 0$ is no longer present. Furthermore, it turns out that in this situation, the densities close to the left boundary quickly approximate a common value ρ_e. The latter is found from conservation of the particle current: $2\rho_e(1 - \rho_e) = J$. We now consider the implications for the phase boundary determined by $x_w = 1$. With $\rho_1^\uparrow(x = 1) = \rho_e$, equation (20) turns into $\rho_e = \beta_{\text{eff}}^\uparrow$, yielding

$$2\beta_{\text{eff}}^\uparrow(1 - \beta_{\text{eff}}^\uparrow) = \alpha_{\text{eff}}^\uparrow(1 - \alpha_{\text{eff}}^\uparrow) + \alpha_{\text{eff}}^\downarrow(1 - \alpha_{\text{eff}}^\downarrow). \tag{22}$$

This condition specifies the phase boundary $x_w = 1$, asymptotically for large Ω. It constitutes a simple quadratic equation in the in and outgoing rates, independent of $\beta^\downarrow$, and contains the set $\alpha^\uparrow = \alpha_{\text{eff}}^\downarrow = \beta^\uparrow$.

5. Stochastic simulations

To confirm our analytic findings from the previous section, we have performed stochastic simulations. The dynamical rules (i)–(iv) described in section 2.1 were implemented using random sequential updating. In our simulations, we have performed averages over typically 10^5 time steps, with $10 \times L$ steps of updating between successive ones. Finite size scaling singles out the analytic solution in the limit of large system sizes, as exemplified in figures 3 and 4.

For all simulations, we have checked that the analytic predictions are recovered upon approaching the mesoscopic limit. We attribute the apparent exactness of our analytic approach in part to the exact current density relation in the steady state of the TASEP [34]. The additional coupling of the two TASEPs in our model is only weak: the local exchange between the two states vanishes in the limit of large system sizes. Correlations between them are washed out, and mean-field is recovered.

The observed exactness of the analytic density profiles within the mesoscopic limit implies that our analytic approach yields exact phase diagrams as well. The latter are the subject of the subsequent section.

6. Two-dimensional phase diagrams

In this section, we discuss the phase behaviour on two-dimensional cuts in the whole five-dimensional parameter space. Already the simplified situation of equal injection rates, $\alpha^\uparrow = \alpha^\downarrow$, yields interesting behaviour. There as well as in the general case, we investigate the role of the spin-flip rate Ω by discussing the situation of small and large values of Ω.

6.1. Equal injection rates

For simplicity, we start our discussion of the phase diagram with equal injection rates, $\alpha^\uparrow = \alpha^\downarrow$. Then, the spin polarization phenomenon, depicted in figure 4, becomes even more striking. Starting from equal densities at the left boundary, and hence zero polarization, spin polarization suddenly switches on at the domain wall position x_w. The particular location of x_w is not triggered by a cue on the track, but tuned through the model parameters.

The phase transitions from LD to the LD–HD_{IN} arising in the IN region take a remarkably simple form. Their location is found from $x_w = 1$, and is determined by equation (20) (if phase coexistence arises for spin-up). Since $\rho^{\uparrow}(x) = \rho^{\downarrow}(x) = \alpha =$ constant for $x < x_w$, equation (20) turns into $\alpha = \beta^{\uparrow}$. The latter transition line intersects the IN–EX boundary, given by $J_{IN} = J_{EX}$, at $\beta^{\uparrow} = \beta^{\downarrow} = \alpha$, i.e. at the point where all entrance and exit rates coincide. At this *multi-critical point* $\mathcal{A}$, a continuous line intersects a discontinuous one. The same transition in the density of spin-down state is, from similar arguments, located at $\alpha = \beta^{\downarrow}$, and also coincides with the IN–EX boundary in $\mathcal{A}$. Neither the multi-critical point $\mathcal{A}$ nor these phase boundaries depend on the magnitude of the gross spin flip rate Ω. Therefore, qualitatively tuning the system's state is possible only upon changing the injection or extraction rates. The other phase transitions within the IN region, namely from the HD to the LD–HD_{IN} phase, are more involved. The analytic solution given by (A.12) and (A.13) has to be considered together with the condition (19) for the transition. However, at the end of section 4.4, we have found that these transitions (determined by $x_w = 0$) disappear for sufficiently large $\Omega > \Omega_C$.

6.1.1. Large values of Ω. In the situation of large $\Omega > \Omega_C$, phase transitions arising from $x_w = 0$ in the IN region or from the analogue in the EX region do not emerge, as discussed at the end of section 4.4. We have drawn resulting phase diagrams in figure 5, showing the phase of spin-up (spin-down) in the left (right) panels, depending on α and $\beta^{\uparrow}$. Along the IN–EX boundary, being the same line (shown as bold) in the left and right panels, a delocalization transition occurs. At the multi-critical point $\mathcal{A}$, it is intersected by continuous lines emerging within the IN resp. the EX region. When $\beta^{\downarrow} > 1/2$, a MC phase emerges in the upper right quadrant, see figures 5(c)–(d).

To illustrate the system's phase behaviour, let us consider what happens along a horizontal line in the phase diagrams (a) and (b), at a value $\beta^{\uparrow} > \beta^{\downarrow}$. At such a line, for small values of α, both spin states are in LD phases. Upon crossing a certain value of α, a domain wall enters at $x_w = 1$ in the spin-down density profile. Then, spin-down exhibits phase coexistence (LD–HD_{IN}), while spin-up remains in a LD phase. Further increasing α, the bold line is reached, where delocalized domain walls arise in both spin states. For larger values of α, a localized domain wall emerges for spin-up (implying a LD–HD_{EX} phase), and a pure HD phase for spin-down. If α is further increased, the domain wall in the spin-up density profile leaves the system through the left boundary (at $x_w = 0$), and pure HD phases remain for both spin states.

While we have found the transitions within the IN region by simple expressions in the previous subsection, the ones emerging in the EX region are more complex and involve the full analytic solutions (A.12) and (A.13). Their most notable feature is that the width of the corresponding coexistence phase decreases with increasing spin-flip rate Ω, until it finally vanishes in the limit $\Omega \to \infty$. This may be seen by considering the analogue of equation (22) in the EX region, which describes the phase boundary as it is asymptotically approached when $\Omega \to \infty$:

$$2\alpha_{\text{eff}}(1 - \alpha_{\text{eff}}) = \beta^{\uparrow}_{\text{eff}}(1 - \beta^{\uparrow}_{\text{eff}}) + \beta^{\downarrow}_{\text{eff}}(1 - \beta^{\downarrow}_{\text{eff}}), \tag{23}$$

it coincides with the IN–EX boundary.

6.1.2. Small values of Ω. As discussed at the end of section 4.4, when $\Omega < \Omega_C$, the appearance of additional phase transitions becomes possible. For example, within the IN region, the situation $x_w = 0$ may emerge. It describes the transition from the HD to the LD–HD_{IN} phase; the analogue

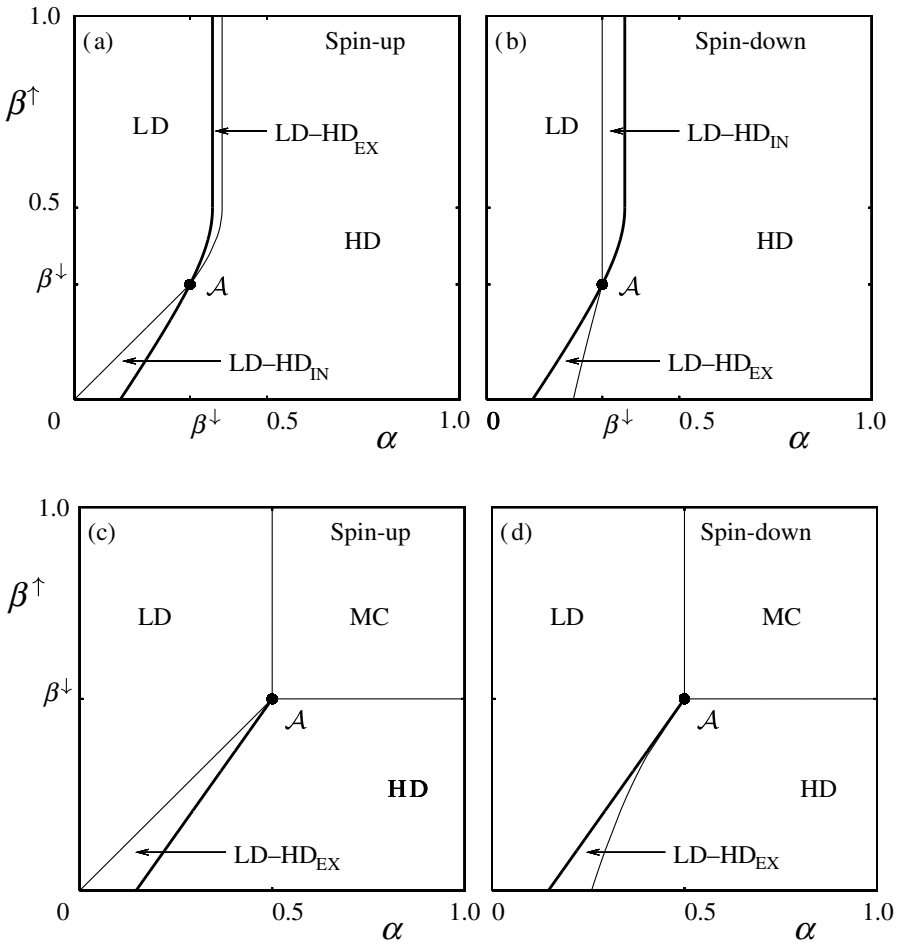

Figure 5. Phase diagrams in the situation of equal entrance rates $\alpha^{\uparrow} = \alpha^{\downarrow} \equiv \alpha$ and large Ω. The phases of the densities of spin-up (spin-down) state are shown in (a) resp. (b) for a value $\beta^{\downarrow} = 0.3$. At a multi-critical point $\mathcal{A}$, continuous lines (thin) intersect with a discontinuous line (bold), the IN–EX boundary. If $\beta^{\downarrow} \geqslant \frac{1}{2}$, the MC phase appears for spin-up, see (c), as well for spin-down, drawn in (d). In the first situation, the switching rate is $\Omega = 0.15$, while $\Omega = 0.2$ in the second.

occurs in the EX region. In figure 6, we show resulting phase diagrams for the spin-up (left panel) and spin-down (right panel), resp. The additional transition lines intersect the IN–EX boundary (bold) at additional multi-critical points $\mathcal{B}_{\mathrm{IN}}$ and $\mathcal{B}_{\mathrm{EX}}$. Also, they partly substitute the IN–EX boundary as a phase boundary: across some parts of the latter, phase transitions do not arise. This behaviour reflects the *decoupling* of the two states for decreasing spin-flip rate Ω. Indeed, for $\Omega \to 0$, the states become more and more decoupled, such that the IN–EX boundary, involving the combined entrance and exit rates of both states, loses its significance.

6.1.3. Multi-critical points. Although the shapes of most of the transition lines appearing in the phase diagrams shown in figure 6 are quite involved, they also exhibit simple behaviour. *Pairwise*, namely one line from a transition in spin-up and another from a related transition in spin-down states, they intersect the IN–EX boundary in the same multi-critical point. This

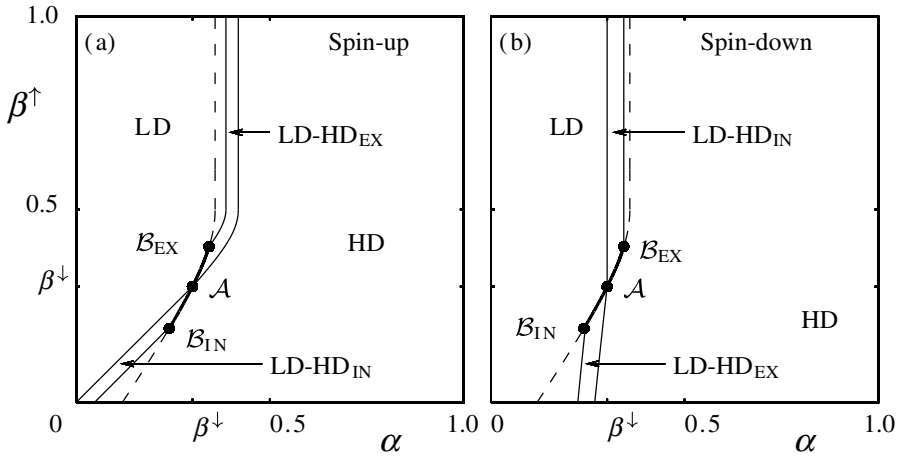

Figure 6. Phase diagrams in the situation of figures 5(a) and (b), but with Ω decreased to a small value, $\Omega = 0.05$. Additional phase transitions emerge in the IN as well as the EX region, accompanied by multi-critical points $\mathcal{B}_{IN}$ and $\mathcal{B}_{EX}$. Caused by them, phase transitions do no longer appear across some parts of the IN–EX boundary, which is there shown as dashed line.

intriguing phenomenon may be understood by considering the multi-critical points: e.g. at $\mathcal{A}$, the transition line from the LD to the LD–HD$_{IN}$ phase in the density profile of spin-up intersects the IN–EX boundary, which implies that there we have a domain wall in the density profile of spin-up at the position $x_w = 1$. However, being on the IN–EX boundary, the condition $J_{IN} = J_{EX}$ implies that in this situation a domain wall forms as well in the density of spin-down states, also located at $x_w = 1$. Consequently, $\mathcal{A}$ also marks the point where the transition line specified by $x_w = 1$ for spin-down states intersects the IN–EX boundary. Due to the special situation of equal entrance rates, one more pair of lines intersects in this point. Similarly, at $\mathcal{B}_{IN}$, the transition line from the HD to LD–HD$_{IN}$ phase in the density profile of spin-up intersects the IN–EX boundary, such that a domain wall forms in the density of spin-up at $x_w = 0$. Again, as $J_{IN} = J_{EX}$ holds on the IN–EX boundary, this implies the formation of a domain wall in the density of spin-down at $x_w = 1$, corresponding to the transition from the LD to the LD–HD$_{EX}$ phase for spin-down in the EX region.

6.2. The general case

Having focused on the physically particularly enlightening case of equal entering rates in the previous subsection, we now turn to the general case. To illustrate our findings, we show phase diagrams depending on the injection and extraction rates for spin-up states, $\alpha^{\uparrow}$ and $\beta^{\uparrow}$. Similar behaviour as for equal entrance rates is observed. The multi-critical point $\mathcal{A}$ now splits up into two distinct points $\mathcal{A}_{IN}$ and $\mathcal{A}_{EX}$.

6.2.1. Large values of Ω: asymptotic results. Again, large Ω prohibit the emergence of the phase transition from the HD to the LD–HD$_{IN}$ phase in the IN region as well as from the LD to the LD–HD$_{EX}$ phase within the EX region, see end of section 4.4. In this paragraph, we consider phase diagrams which are approached asymptotically when $\Omega \to \infty$. Convergence is fast in Ω, and the asymptotic phase boundaries yield an excellent approximation already for $\Omega \gtrsim 2\Omega_C$.

The transition from LD to the LD–HD_{IN} phase in the IN region asymptotically takes the form of equation (22), and the one from HD to the LD–HD_{EX} phase in the EX region is obtained by particle–hole symmetry. All phase boundaries, including the IN–EX boundary, are thus given by simple quadratic expressions.

Phase diagrams with different topologies that can emerge are exhibited in figures 7 and 8. As in the previous subsection, we show the phases of spin-up (spin-down) states on the left (right) panels. The phase boundaries between the LD and the LD–HD_{IN} phase in the IN region for spin-up as well as spin-down both intersect the IN–EX boundary in a multi-critical point $\mathcal{A}_{IN}$, being located at $\beta^{\uparrow} = \beta^{\downarrow}$. Similarly, the lines of continuous transitions within the EX region both coincide with the IN–EX boundary in a multi-critical point $\mathcal{A}_{EX}$, which is situated at $\alpha^{\uparrow} = \alpha^{\downarrow}$. Note that the phase transitions emerging in the density profile of spin-down within the IN region do not depend on $\beta^{\uparrow}$, thus being horizontal lines in the phase diagrams. Within the EX region they are independent of $\alpha^{\uparrow}$, yielding vertical lines.

For $\alpha^{\downarrow}, \beta^{\downarrow} < 1/2$, figure 7 shows different topologies of phase diagrams, which only depend on which of the multi-critical points $\mathcal{A}_{IN}$, $\mathcal{A}_{EX}$ is present. If both appear, see figure 7(a) and (b), the LD–HD_{IN} and the LD–HD_{EX} phase for spin-up are adjacent to each other, separated by the IN–EX boundary. Although in both phases localized domain walls emerge, their position changes discontinuously upon crossing the delocalization transition. For example, starting within the LD–HD_{IN} phase, the domain wall delocalizes when approaching the IN–EX boundary, and, having crossed it, relocalizes again, but at a different position.

When $\alpha^{\downarrow} = \beta^{\downarrow} < 1/2$, a subtlety emerges, see figures 8(a) and (b). If both $\alpha^{\uparrow} \geqslant 1/2$ and $\beta^{\uparrow} \geqslant 1/2$, i.e. in the upper right quadrant of the phase diagrams, these rates effectively act as $1/2$, and the condition $J_{IN} = J_{EX}$ for the IN–EX boundary is fulfilled *in this whole region*. Therefore, delocalized domain walls form on both lanes within this region, as is confirmed by our stochastic simulations [31].

The MC phase emerges when all rates exceed or equal the value $1/2$, corresponding to the upper left quadrant of the phase diagrams in figures 8(c) and (d).

6.2.2. Small values of Ω. When $\Omega < \Omega_C$, the transitions from LD to LD–HD_{IN} within the IN region as well as the analogue in the EX region are possible. As in the case of equal entering rates, the corresponding transition lines pairwise intersect the IN–EX boundary in multi-critical points $\mathcal{B}_{IN}$ and $\mathcal{B}_{EX}$. As all transitions between phases of the spin-down density within the IN region are independent of $\beta^{\uparrow}$, the corresponding lines are simply horizontal; and within the EX region, their independence of $\alpha^{\uparrow}$ implies that they yield vertical lines. The phase diagram for the density of spin-down is thus easily found from the IN–EX boundary given by $J_{IN} = J_{EX}$ together with the locations of the multi-critical points $\mathcal{A}_{IN}$, $\mathcal{A}_{EX}$, $\mathcal{B}_{IN}$ and $\mathcal{B}_{EX}$. The latter follow from the intersection of phase transition lines for the density of spin-up, involving the whole analytic solution (A.12) and (A.13), with the IN–EX boundary.

In figure 9 two interesting topologies that may arise are exemplified. Induced by the presence of the multi-critical point $\mathcal{B}_{IN}$, phase transitions do not occur across all the IN–EX boundary, which is then only shown as dashed line. In figures 9(a) and (b), the points $\mathcal{A}_{EX}$ and $\mathcal{B}_{IN}$ are present. The LD–HD_{IN} phase for spin-up intervenes the LD and the HD phase; the LD–HD_{EX} phase for spin-up is also present, though very tiny. In the phase diagram of spin-down, the LD–HD_{IN} phase intervenes the LD and the HD phase accompanied by continuous as well as discontinuous transitions. Again, the presence of the multi-critical points induces the topology;

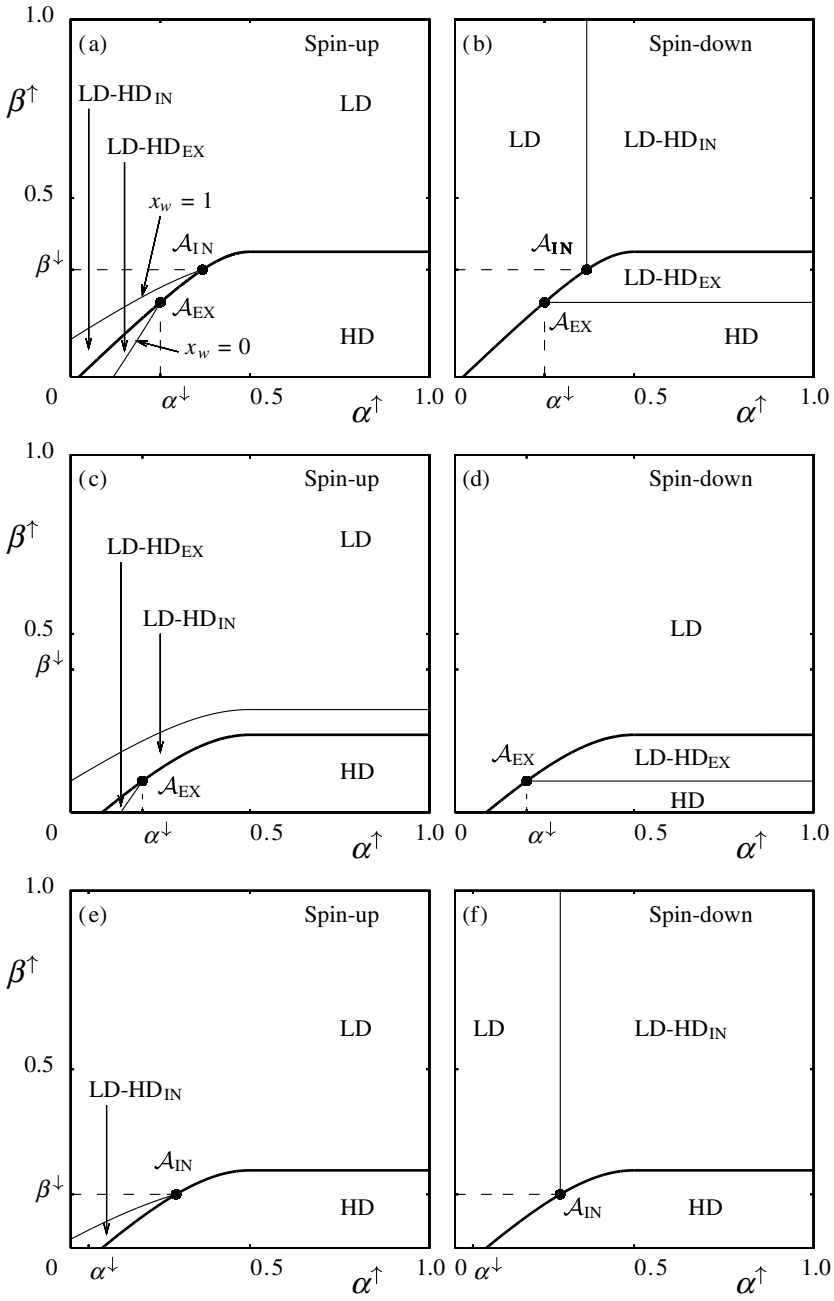

Figure 7. Phase diagrams in the general situation: asymptotic results for large Ω. Lines of continuous transitions (thin) within the IN resp. EX region intersect the delocalization transition line (bold) in multi-critical points $\mathcal{A}_{IN}$ resp. $\mathcal{A}_{EX}$. Both of these points appear in (a) and (b) ($\alpha^\downarrow = 0.25$, $\beta^\downarrow = 0.3$) while only $\mathcal{A}_{EX}$ is present in (c) and (d) ($\alpha^\downarrow = 0.2$, $\beta^\downarrow = 0.4$) and $\mathcal{A}_{IN}$ alone in (e) and (f) ($\alpha^\downarrow = 0.05$, $\beta^\downarrow = 0.15$), yielding different topologies.

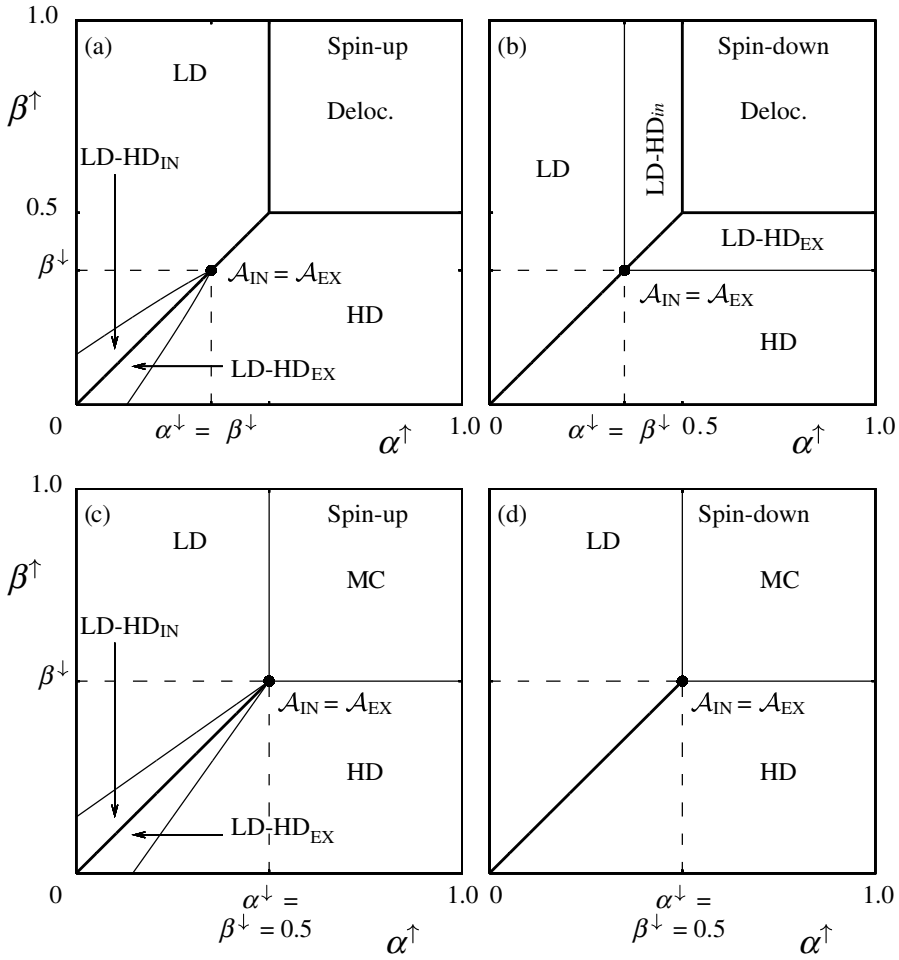

Figure 8. Delocalization as well as MC. When $\alpha^\downarrow = \beta^\downarrow < 1/2$ and $\alpha^\uparrow, \beta^\uparrow \geqslant 1/2$ (upper right quadrant in (a) and (b)), delocalized domain walls form in the density profiles of both spin states. If instead $\alpha^\downarrow, \beta^\downarrow \geqslant 1/2$, the MC phase emerges, see (c) and (d).

e.g. in figures 9(c) and (d), only $\mathcal{B}_{IN}$ appears. For the discussion of the possible topologies, we encounter the restriction that $\mathcal{A}_{IN}$ and $\mathcal{B}_{IN}$ cannot occur together, as well as $\mathcal{A}_{EX}$ and $\mathcal{B}_{EX}$ exclude each other (otherwise, the lines determined by $x_w = 0$ and $x_w = 1$ would cross).

We now discuss the influence of the spin-flip rate Ω on the continuous transition lines for spin-up. In section 4.4 the manifold defined by $\alpha^\uparrow = \beta^\uparrow = \alpha^\downarrow_{eff}$ was found to be a sub-manifold of the phase boundary specified by $x_w = 1$ in the IN region. Independent of Ω, the point $\alpha^\uparrow = \beta^\uparrow = \alpha^\downarrow_{eff}$, denoted by $\mathcal{N}_{IN}$, thus lies on the boundary between the LD and the LD–HD$_{IN}$ phase (determined by $x_w = 1$). For large Ω, this boundary approaches the one given by equation (22).

Regarding the transition from the HD to the LD–HD$_{IN}$ within the IN region (determined by $x_w = 0$), section 4.4 revealed that for increasing Ω it leaves the IN region at a critical transfer rate $\Omega^*(\alpha^\downarrow, \beta^\uparrow)$. In the limit $\Omega \to 0$, the densities $\rho^\uparrow(x)$ and $\rho^\downarrow(x)$ approach constant values, and both the curve $x_w = 1$ as $x_w = 0$ for spin-up in the IN region approach the line $\beta^\uparrow = \alpha^\uparrow$ for

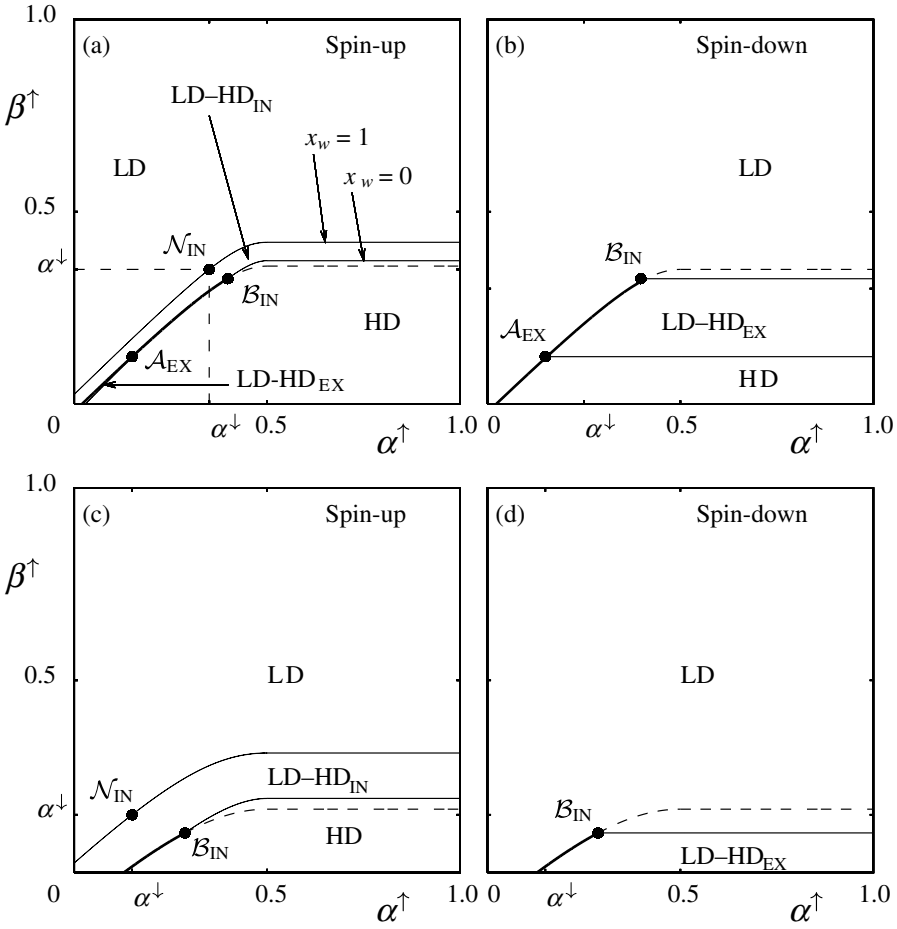

Figure 9. Phase diagrams in the general case and small values of Ω. The nodal point $\mathcal{N}_{IN}$ remains unchanged when Ω is varied. The appearance of the multi-critical point $\mathcal{B}_{IN}$ is accompanied by the non-occurrence of phase transitions across parts of the IN–EX boundary, then shown as dashed line. The multi-critical point $\mathcal{A}_{EX}$ emerges in (a) and (b), but not in the situation of (c) and (d). Parameters are $\Omega = 0.08$, $\alpha^{\downarrow} = 0.35$, $\beta^{\downarrow} = 0.45$ in (a) and (b) and $\Omega = 0.2$, $\alpha^{\downarrow} = 0.15$, $\beta^{\downarrow} = 0.4$ in (c) and (d).

$\alpha^{\uparrow} \leqslant \frac{1}{2}$. The phase in the upper right quadrant in the phase diagram converges to the MC phase, such that in this limit, the case of two uncoupled TASEPs is recovered.

7. Conclusions

We have presented a detailed study of an exclusion process with internal states recently introduced in [19]. The TASEP has been generalized by assigning two internal states to the particles. Pauli's exclusion principle allows double occupation only for particles in different internal states. Occasional switches from one internal state to the other induce a coupling between the transport processes of the separate states. Such a dynamics encompasses diverse situations, ranging from vehicular traffic on multiple lanes to molecular motors walking on intracellular tracks and future spintronics devices.

We have elaborated on the properties of the emerging non-equilibrium steady state focusing on density and current profiles. In a mesoscopic scaling of the switching rate between the internal states, nontrivial phenomena emerge. A localized domain wall in the density profile of one of the internal states induces a spontaneous polarization effect when viewing the internal states as spins. We provide an explanation based on the weakly conserved currents of the individual states and the current-density relations. A quantitative analytic description within a mean-field approximation and a continuum limit has been developed and solutions for the density and current profiles have been presented. A comparison with stochastic simulations revealed that our analytic approach becomes exact in the limit of large system sizes. We have attributed this remarkable finding to the exact current-density relation in the TASEP, supplemented by the locally weak coupling of the two TASEPs appearing in our model: $\omega \to 0$ in the limit of large system sizes. Local correlations between the two internal states are thus obliterated, as particles hop forward on a much faster time-scale than they switch their internal state.

Furthermore, the parameter regions that allow for the formation of a localized domain wall have been considered. Analytic phase diagrams for various scenarios, in particular the case of equal entrance rates, have been derived. The phase diagrams have been found to exhibit a rich structure, with continuous as well as discontinuous non-equilibrium phase transitions. The discontinuous one originates in the conserved particle current, which is either limited by injection or extraction of particles. At the discontinuous transition between both regimes, delocalized domain walls emerge in the density profiles of *both* internal states. Multi-critical points appear at the intersections of different transition lines organizing the topology of the phase diagrams. Two classes of multi-critical points are identified, one of them arises only for sufficiently small gross spin-flip rate $\Omega < \Omega_C$. The value Ω_C, calculated analytically, provides a natural scale for the rate Ω.

It would be of interest to see which of the described phenomena qualitatively remain when generalizing the model to include more than two internal states. Indeed, within the context of molecular motors walking on microtubuli [7], between 12 and 14 parallel lanes are relevant. Also, the internal states might differ in the sense of different switching rates from one to another [28] and the built-in asymmetry may result in different phases. In the context of intracellular transport it appears worthwhile to investigate the consequences of a coupling to a bulk reservoir, cf [29, 30, 35]; in particular, to study the interplay of domain wall formation induced by attachment and detachment processes as well as rare switching events.

Acknowledgments

We are grateful for helpful discussions with Felix von Oppen, Ulrich Schollwöck, Paolo Pierobon and Mauro Mobilia. Financial support of the German Excellence Initiative via the program 'Nanosystems Initiative Munich (NIM)' is gratefully acknowledged.

Appendix A. The densities in the first order approximation and the critical value Ω_C

In this appendix, we give details on the derivation of the analytic solution of the mean-field approximation in the continuum limit to first-order in ϵ, i.e. the system of differential equations (10) and (11).

Summing them we find

$$\partial_x[2\rho^{\uparrow}(x_i) - 1]^2 + \partial_x[2\rho^{\downarrow}(x_i) - 1]^2 = 0, \tag{A.1}$$

such that

$$[2\rho^{\uparrow}(x_i) - 1]^2 + [2\rho^{\downarrow}(x_i) - 1]^2 = J, \tag{A.2}$$

constitutes a first integral. Remember that

$$j^{\mathrm{tot}} = \rho^{\uparrow}(x_i)[1 - \rho^{\uparrow}(x_i)] + \rho^{\downarrow}(x_i)[1 - \rho^{\downarrow}(x_i)],$$

such that J is given by the total current:

$$J = 2 - 4j^{\mathrm{tot}}. \tag{A.3}$$

This equation suggests the following parameterization:

$$\cos\theta = J^{-1/2}(2\rho^{\uparrow} - 1), \qquad \sin\theta = J^{-1/2}(2\rho^{\downarrow} - 1). \tag{A.4}$$

The derivative reads

$$\frac{\sqrt{J}}{2}\cos\theta\frac{\mathrm{d}\theta}{\mathrm{d}x} = \frac{\mathrm{d}\rho^{\uparrow}}{\mathrm{d}x}, \tag{A.5}$$

which leads to the differential equation

$$\sqrt{J}\sin\theta\cos\theta\frac{\mathrm{d}\theta}{\mathrm{d}x} = \Omega(\sin\theta - \cos\theta). \tag{A.6}$$

This may be solved by a separation of variables:

$$\frac{\Omega}{\sqrt{J}}x = \int_{\theta(0)}^{\theta(x)} \frac{\sin\theta\cos\theta}{\sin\theta - \cos\theta}\,\mathrm{d}\theta. \tag{A.7}$$

To perform the integral, the substitution $y = \tan\theta/2$ is useful. We obtain the inverse function $x = x(\theta)$:

$$x(\theta) = \frac{\sqrt{J}}{\Omega}G(y)\Big|_{y=\tan(\theta/2)} + I. \tag{A.8}$$

Here we defined the function $G(y)$ by

$$G(y) = \left\{\frac{1+y}{1+y^2} + \frac{\sqrt{2}}{4}\ln\left|\frac{\sqrt{2} - (1+y)}{\sqrt{2} + 1 + y}\right|\right\}, \tag{A.9}$$

and I is an constant of integration.

To obtain the inverse functions $x(\rho^{\uparrow})$ and $x(\rho^{\downarrow})$, we have to express $\tan\frac{\theta}{2}$ by $\rho^{\uparrow}$ resp. $\rho^{\downarrow}$. Recognize that $\tan\frac{\theta}{2}$ can be positive or negative. We therefore define

$$s^{\downarrow} = \begin{cases} -1 & \text{if } \rho^{\downarrow} < \frac{1}{2} \\ +1 & \text{if } \rho^{\downarrow} > \frac{1}{2} \end{cases}, \tag{A.10}$$

and analogously $s^{\uparrow}$ with $\uparrow$ and $\downarrow$ interchanged. Now

$$\tan\frac{\theta}{2} = s^{\downarrow}\sqrt{\frac{1 - J^{-1/2}(2\rho^{\uparrow} - 1)}{1 + J^{-1/2}(2\rho^{\uparrow} - 1)}}. \tag{A.11}$$

The inverse functions $x(\rho^{\uparrow})$ and $x(\rho^{\downarrow})$ thus read:

$$x(\rho^{\uparrow}) = \frac{\sqrt{J}}{\Omega}G(y)\Big|_{y=s^{\downarrow}\sqrt{\frac{1-J^{-1/2}(2\rho^{\uparrow}-1)}{1+J^{-1/2}(2\rho^{\uparrow}-1)}}} + I, \tag{A.12}$$

$$x(\rho^{\downarrow}) = \frac{\sqrt{J}}{\Omega}G(y)\Big|_{y=s^{\uparrow}\sqrt{\frac{1-J^{-1/2}(2\rho^{\downarrow}-1)}{1+J^{-1/2}(2\rho^{\downarrow}-1)}}} + I. \tag{A.13}$$

The constants of integration I and $J = 2 - 4j^{\mathrm{tot}}$ are determined by matching the boundary conditions. The inverse functions of equations (A.12) and (A.13) constitute the solution to equations (10) and (11), within the first-order approximation to the mean-field equations for the densities in the continuum limit.

Next, we derive the result on Ω_{C} given at the end of section 4.4. Therefore, consider figure 4. We are interested in the point $x_{1/2}$, and thus in the right branch of the spin-up density profile. As the spin-down density is in the LD phase, i.e. it is smaller than $\frac{1}{2}$, we have $s^{\downarrow} = -1$ in the above solution for $\rho^{\uparrow}$. Thus, $y \leqslant 0$ in equation (A.12). At the branching point of the analytic solution, i.e. the point $x_{1/2}$, we have the density $\frac{1}{2}$, such that there $y = -1$, implying $G(y) = 0$. Now, if this branching point lies on the right boundary, $x_{1/2} = 0$, as it does for the critical Ω^{*}, this yields $I = 0$ in equation (A.12). On the other hand, the right branch satisfies the boundary condition on the right: $\rho^{\uparrow}(x = 1) = 1 - \beta^{\uparrow}$. Upon substitution into equation (A.12), we obtain

$$1 = x(1 - \beta^{\uparrow}) = \frac{\sqrt{J}}{\Omega^{*}}G(y)\Big|_{y=-\sqrt{\frac{1-J^{-1/2}(1-2\beta^{\uparrow})}{1+J^{-1/2}(1-2\beta^{\uparrow})}}}. \tag{A.14}$$

which for given $\alpha^{\downarrow}$, $\beta^{\uparrow}$ is an equation for $\Omega^{*}(\alpha^{\downarrow}, \beta^{\uparrow})$. In particular, $\Omega^{*}(\alpha^{\downarrow}, \beta^{\uparrow})$ is monotonically increasing in G. Investigating $G(y)$, it turns out that $G(y)$ is in turn increasing in y. Since y is bounded from above by $y = 0$, the maximal value for $G(y)$ is provided by $G(y = 0) = 1 + \frac{1}{4}\sqrt{2}\ln(3 - 2\sqrt{2})$. Next, we note that $\Omega^{*}(\alpha^{\downarrow}, \beta^{\uparrow})$ is an increasing function of $\sqrt{J}$. With the constraint that $\alpha^{\uparrow}_{\mathrm{eff}} = \frac{1}{2}$, which is necessary for $x_{1/2} = 0$, the largest $\sqrt{J}$ arises for $\alpha^{\downarrow} = 0$, i.e. $\sqrt{J} = 1$. Combining both results, the maximal value for the critical rates $\Omega^{*}(\alpha^{\downarrow}, \beta^{\uparrow})$ occurs for $\alpha^{\downarrow} = 0$ and $y = 0$. Both conditions together yield

$$\Omega_{\mathrm{C}} = 1 + \tfrac{1}{4}\sqrt{2}\ln(3 - 2\sqrt{2}). \tag{A.15}$$

Finally, we note that $\alpha^{\downarrow} = 0$ and $y = 0$ implies $\beta^{\uparrow} = 0$, such that Ω_{C} arises if $\alpha^{\downarrow} = 0$ and $\beta^{\uparrow} = 0$.

References

[1] Barabasi A and Stanley H 1995 *Fractal Concepts in Surface Growth* (Cambridge: Cambridge University Press)
[2] Deutscher G, Zallan R and Adler J (ed) 1983 *Percolation Structures and Processes* (*Annals of the Israel Physical Society* vol 5) (Bristol: Adam Hilger)
[3] Droz M, Rácz Z and Schmidt J 1989 *Phys. Rev.* A **39** 2141
[4] Mattis D C and Glasser M L 1998 *Rev. Mod. Phys.* **70** 979
[5] Schmittmann B and Zia R 1995 *Phase Transitions and Critical Phenomena* vol 17, ed C Domb and J Lebowitz (London: Academic)
[6] MacDonald C, Gibbs J and Pipkin A 1968 *Biopolymers* **6** 1
[7] Howard J 2001 *Mechanics of Motor Proteins and the Cytoskeleton* (Sunderland: Sinauer)
[8] Hirokawa N 1998 *Science* **279** 519
[9] Helbing D 2001 *Rev. Mod. Phys.* **73** 1067
[10] Chowdhury D, Santen L and Schadschneider A 2000 *Phys. Rep.* **329** 199
[11] Derrida B and Evans M 1997 *Nonequilibrium Statistical Mechanics in One Dimension* ed V Privman (Cambridge: Cambridge University Press) pp 277–304
[12] Mukamel D 2000 *Soft and Fragile Matter* ed M Cates and M Evans (Bristol: Institute of Physics Publishing) pp 237–58
[13] Schütz G 2001 *Phase Transitions and Critical Phenomena* vol 19, ed C Domb and J Lebowitz (San Diego: Academic) pp 3–251
[14] Krug J 1991 *Phys. Rev. Lett.* **67** 1882
[15] Odor G 2004 *Rev. Mod. Phys.* **76** 663
[16] Täuber U C, Howard M J and Hinrichsen H 1998 *Phys. Rev. Lett.* **80** 2165
[17] Noh J D and Park H 2005 *Phys. Rev. Lett.* **94** 145702
[18] Dagotto E and Rice T M 1996 *Science* **271** 618
[19] Reichenbach T, Franosch T and Frey E 2006 *Phys. Rev. Lett.* **97** 050603
[20] Zutic I, Fabian J and Sarma S D 2004 *Rev. Mod. Phys.* **76** 323
[21] Hahn C K, Park Y J, Kim E K and Min S 1998 *Appl. Phys. Lett.* **73** 2479
[22] Hinsch H, Kouyos R and Frey E 2006 *Traffic and Granular Flow '05* ed A Schadschneider, T Pöschel, R Kühne, M Schreckenberg and D E Wolf (Berlin: Springer)
[23] Popkov V and Peschel I 2001 *Phys. Rev.* E **64** 026126
[24] Popkov V and Schütz G M 2003 *J. Stat. Phys.* **112** 523
[25] Popkov V 2004 *J. Phys. A: Math. Gen.* **37** 1545
[26] Pronina E and Kolomeisky A B 2004 *J. Phys. A: Math. Gen.* **37** 9907
[27] Mitsudo T and Hayakawa H 2005 *J. Phys. A: Math. Gen.* **38** 3087
[28] Pronina E and Kolomeisky A B 2006 *Physica* A **372** 12
[29] Parmeggiani A, Franosch T and Frey E 2003 *Phys. Rev. Lett.* **90** 086601
[30] Parmeggiani A, Franosch T and Frey E 2004 *Phys. Rev.* E **70** 046101
[31] Reichenbach T, Franosch T and Frey E in preparation
[32] Shaw L B, Zia R K P and Lee K H 2003 *Phys. Rev.* E **68** 021910
[33] Pierobon P, Franosch T and Frey E 2006 *Phys. Rev.* E **74** 031920
[34] Derrida B 1998 *Phys. Rep.* **301** 65
[35] Klumpp S and Lipowsky R 2003 *J. Stat. Phys.* **113** 233